

Effects of Spraying Parameters on Phase Formation and Distribution in Plasma-Sprayed Hydroxyapatite Coatings

L. Sun, C.C. Berndt, R.S. Lima, A. Kucuk
SUNY at Stony Brook, Stony Brook, New York, USA

K.A. Khor
Nanyang Technological University, Nanyang, Singapore

Abstract

Calcined spraydried hydroxyapatite ($\text{Ca}_{10}(\text{PO}_4)(\text{OH})_6$; i.e., HA) powders were atmospherically plasma sprayed (APS) using various process parameters. The resulting phases within the coating **surface** and the interface between the coating and the substrate were analyzed using X-ray diffraction (XRD) methods. This XRD revealed the presence of both amorphous (i.e., amorphous calcium phosphate: ACP) and crystalline phases. The crystalline phases included both HA and some impurity phases from the decomposition of HA, such as tricalcium phosphate (α -TCP and β -TCP), tetracalcium phosphate (TTCP) and calcium oxide (CaO). The crystallinity of HA decreased with increasing spray power and stand-off distance (SOD). The percentage of all impurity phases increased with the spray power. The percentage of both TCP and TTCP decreased with the SOD while the CaO percentage increased. In addition, the percentage of ACP and CaO were higher in the interface than at the surface of the coating while the percentage of TCP and TTCP exhibited the opposite effect.

Introduction

Hydroxyapatite (HA) has been used as an implant material due to its good biocompatibility and bioactivity as well as its compositional similarity to inorganic bone. Due to the poor mechanical properties of bulk HA in load-bearing situations, HA was generally used as a coating on a metallic **substrate**.^{1,2} Plasma spraying is one of the most popular methods to apply the coating onto metals. However, due to the extremely high temperature of the plasma flame and the rapid cooling rate, the composition and the structure of the HA coatings are greatly changed from those of the original powders. HA powders may be melted, with some of the melt becoming amorphous calcium phosphate (ACP) upon impacting the substrate, or becoming dehydroxylated **and/or decomposed** during the spray process. It was found that the crystallinity of the HA coating **decreased** while some impurity phases such as **alpha-**

tricalcium phosphate (α - $\text{Ca}_2(\text{PO}_4)_3$, α -TCP), **beta-tricalcium phosphate** (β - $\text{Ca}_2(\text{PO}_4)_3$, β -TCP), tetracalcium phosphate ($\text{Ca}_4\text{P}_2\text{O}_9$, TTCP) and calcium oxide (CaO) appeared after **spraying**.^{3,4,5}

Previous studies have indicated that the bone response to the HA coatings and subsequent bone growth were dominantly affected by the crystallinity and the phase purity of the HA coatings due to the faster dissolution rate of the amorphous phase and some of the impurity phases in body **fluids**.^{6,7,8,9} Therefore, to obtain HA coatings with predictable properties for actual implant application, the crystallinity and the phase purity of the HA coatings should be effectively designed. To achieve this, both the spray parameters and the properties of the original HA feedstock should be strictly controlled.

In this study, calcined spray-dried HA powders were used as the feedstock. The crystallinity and impurity phases of the HA coatings were evaluated with regard to the spray parameters and quantitatively assessed using a fitting program. In addition, the percentage of the amorphous phase and the impurity phases in the surface and the interface (between coating and substrate) of HA coatings were compared using identical quantitative methods.

Experimental

Feedstock. The HA powders were produced by reacting orthophosphoric acid (H_3PO_4) with calcium hydroxide ($\text{Ca}(\text{OH})_2$) followed by spray drying at around **200°C** and heat treatment at **800°C** for 3 hours. The heat treatment was used to calcine the agglomerated powders. The powders were then sieved to less than 100 μm to ensure uniform melting and deposition during the plasma spray process. The morphology of the powders was examined using a **Philips** ISI-SX-30 Scanning Electron Microscope (SEM) and the particle size distribution was evaluated using a Honeywell Microtrac **SRA** Particle Analyzer.

Plasma Spraying. The calcined spraydried HA powders were atmospherically plasma sprayed (APS) using a **Metco** 3MB plasma torch with a GH nozzle (Sulzer-Metco, Westbury, NY). Argon was used as both the primary gas (at 50 slpm) and carrier gas (at 3.65 slpm), and hydrogen as the secondary gas. The volume of the

hydrogen was adjusted to obtain different spray voltage. Two arc currents and stand-off distances (SOD) were selected. The mild steel substrate was grit-blasted and cleaned with acetone before spraying. Some of the substrates were lightly grit blasted to permit easy coating removal from the substrate after spraying. The powder feed rate was 14 g/min. (Note: When the powder feed rate was changed from 14 g/min to 20 g/min with other parameters remaining the same, although the deposition efficiency increased 5-10%, no obvious difference was revealed in the XRD patterns, so the effects of powder feed rate will not be discussed.) All coatings with substrates (sample 1-6) were sprayed for 3 passes, and all peel-off coatings (sample 1p, 2p, 5p and 6p) were sprayed for 15 passes. The thickness of the coating varied from 75 μm to 600 μm as a result of different spray passes and deposition efficiencies. The various process parameters used are shown in Table 1.

Table 1 Plasma Spray Parameters

Sample type	Spray current (A)	Spray voltage (V)	Secondary gas (H ₂ , slm)	Stand-off distance (mm)
1/1p	500	55	5.6	80
2/2p	500	55	5.6	160
3	500	70	11	80
4	600	60	5.6	80
5/5p	600	70	11	80
6/6p	600	70	11	160

X-ray Diffraction and Quantitative Analysis X-ray diffraction was performed on both the feedstock and the plasma sprayed HA coatings (both the surface and interface in the case of peel-off coatings) using a computer controlled Philips PW 1729 X-ray diffractometer with CuKα₁ radiation; the operating voltage was 40 kV and current 30 mA. The goniometer was set at a scan rate of 0.005 °/sec over a 2θ range of 20-60°. The peaks were identified by comparing with the standard JCPDS (Joint Committee on Powder Diffraction Standard) cards¹⁰ (as shown in Table 2).

To evaluate the crystallinity and purity of the HA coatings, the following quantitative phase analysis methods were revised from some previous studies,^{3,11,12,13} with the intent to give a quick and reasonable estimation of the percentage of the amorphous phase and impurity phases within HA coatings and their relationship with the spray parameters used.

Table 2 Most intense peaks of crystalline phases in plasma sprayed HA coatings

Phase	peak	2θ°	JCPDS No.
Ca ₁₀ (PO ₄)(OH) ₆ , HA	(211)	31.8	9-432
α-Ca ₂ (PO ₄) ₃ , α-TCP	(170)	30.7	9-348
β-Ca ₂ (PO ₄) ₃ , β-TCP	(0.2.10)	31.0	9-169
Ca ₄ P ₂ O ₃ , TTCP	(040)	29.7	25-1137
CaO	(200)	37.4	4-777

Curve fitting was performed by fitting the most intense peak of each crystalline phase (as shown in Table 2) and the amorphous hump in the range of 25-37° (2θ). The ACP/HA ratio and the impurity phases to HA ratios (i.e., TCP/HA, TTCP/HA, CaO/HA) were calculated using Equations 1 and 2 respectively:

$$ACP/HA = \frac{A_{ACP}}{3.23 * A_{HA}} \quad (1)$$

$$TCP/HA = \frac{A_{TCP}}{A_{HA}} \quad (2)$$

In Eq. 1, A_{ACP} is the integrated intensity of the ACP phase, which was evaluated using the area of the amorphous hump between 25° and 37°. The term "3.23*A_{HA}" is the total integrated intensity of all HA peaks within 25-37°. A_{HA} is the area of the most intense (211) peak of HA, and the factor 3.23 is the ratio of the total intensity of all HA peaks in a 2θ range of 25-37° in JCPDS card (9-432) to the intensity of the (211) peak. In Eq. 2, A_{TCP} is the area of the most intense peaks of both α-TCP and β-TCP since these two peaks are very close. TTCP/HA and CaO/HA can be calculated using Eq. 2 by replacing A_{TCP} with A_{TTCP} and A_{CaO}, which are respectively the area of the most intense peak of TTCP and CaO. This quantitative analysis method was based on the assumption that the scattering factors for all phases within HA coatings are similar." It is estimated that the relative error in the above calculation is within five percent of the mean value.

The percentage of HA and ACP within the HA coatings can, thus, be calculated as follows:

$$HA\% = \frac{1}{1 + ACP/HA + TCP/HA + TTCP/HA + CaO/HA} \times 100\% \quad (3)$$

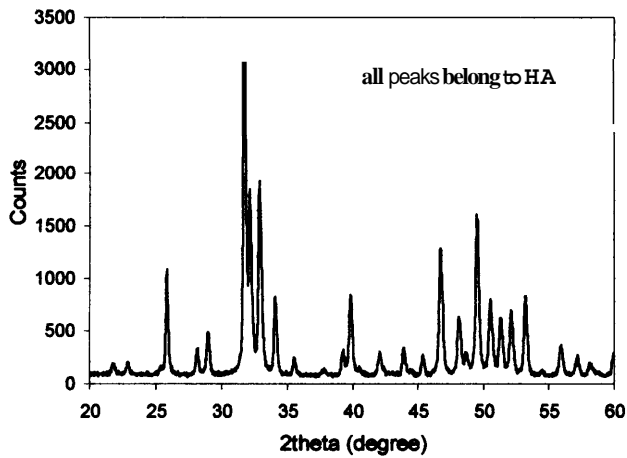
$$ACP\% = HA\% \times ACP/HA \quad (4)$$

The percentage of TCP, TTCP and CaO (i.e., TCP%, TTCP%, CaO%) can be calculated using Eq. 4 by replacement of the "ACP" and "ACP/HA" term.

The crystallinity of the HA coating can be evaluated using the ACP percentage obtained above while the purity of the HA coating can be evaluated using the percentage of each impurity phase.

Results and Discussion

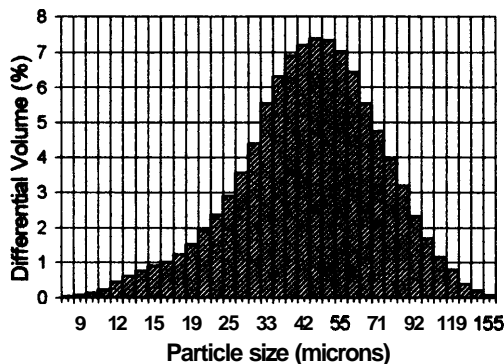
Powder Characterization. The feedstock powders are fully crystallized pure HA phase as shown in Fig. 1(a). The SEM morphology of the HA powders (Fig. 1(b)) shows that the particles are quite spherical, while each particle is agglomerated by many fine particles. The particle size distribution of the HA powders was found mainly within 15 to 100 μm with the average at around 45 μm.



(a) XRD pattern



(b) SEM morphology



(c) Particle size distribution

Figure 1. Characterization of calcined spray dried hydroxyapatite powders

Effects of spray power and SOD. XRD patterns of the HA coatings sprayed at different power levels are shown in Fig. 2. When the spray power was increased from 27.5 kW to 35 kW, the overall intensity of HA peaks decreased and the amorphous hump became more obvious. As well, the peaks of

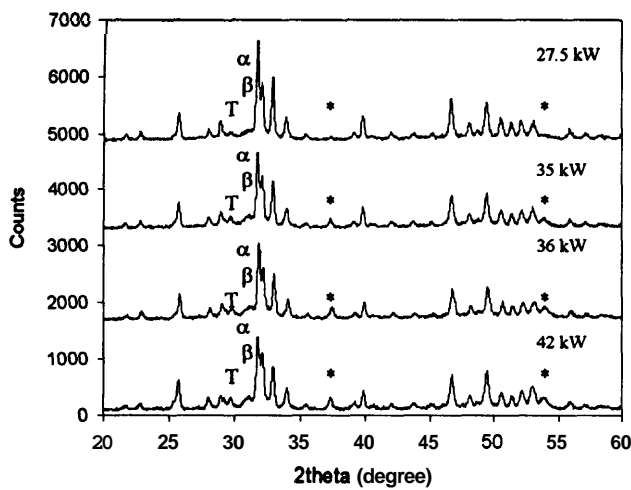
impurity phases (α -TCP, β -TCP, TTCP and CaO) also increased. However, the phases in HA coatings did not show much change when the spray power was further increased to 42 kW. By comparing the XRD patterns of HA coatings sprayed at the same power level but different SOD, it can be seen that the intensity of all HA peaks decreased appreciably and the amorphous hump became very obvious when the SOD was increased from 80 mm to 160 mm. The peaks of impurity phases, specifically the peaks of CaO, became significant when both spray power and SOD reached their highest values.

In addition to the effects on the phase composition in HA coatings, when the SOD was increased from 80 mm to 160 mm, the thickness of the coating decreased and the deposition efficiency was ~ 60% of the former. The change of spray power, however, did not show any obvious influence on the deposition efficiency.

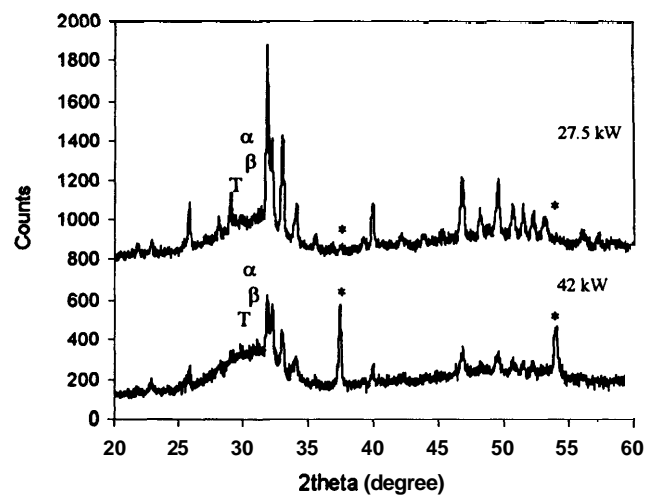
The effects of spray power and SOD on the crystallinity and purity of HA coatings can be quantitatively evaluated using the procedures introduced before. Several quantitative analysis methods have been used previously to characterize the crystallinity and/or purity of HA coatings, such as the direct intensity ratio method,^{11,14} an internal standard method^{12,13,15} and curve fitting of the amorphous hump.^{3,11,13} The internal standard method would be able to give more precise phase percentage if the integrated intensity of all peaks of each phase within the XRD spectrum were measured and some calibration curves were established.¹⁶ Practically, however, as most peaks of α -TCP, β -TCP, TTCP and HA itself overlap each other and a pure amorphous HA is difficult to prepare, the data obtained from this method may not represent the real phase percentage despite a lot of time and work needed. The intent of the analysis presented here is to characterize the crystallinity and different types of impurity phases within HA coatings and to assess their relationship with respect to the spray parameters.

Effects on Crystallinity. As shown in Fig. 3, the ACP percentage of HA coatings increased with the increase of spray power and increased significantly when the SOD increased from 80 mm to 160 mm. It is known that during spraying, some of the HA particles are melted and when they impact on the metallic substrate or the already formed coating, some of these melted portions recrystallized while most of them solidified into amorphous phase due to the high cooling rate and high degree of dehydroxylation.¹⁵ When the input power was increased, the heat content of the plasma became higher and more particles were melted. As a result, more ACP phase formed. In addition, since the temperature of the plasma was higher, the cooling rate and dehydroxylation also became higher, which also promoted the formation of the ACP phase. As it can be seen from Fig. 3, when the spray power was further increased from 35 kW to 42 kW, the ACP percentage almost remained the same as was also found in Tsui et al's work. This probably can be explained due to the low thermal conductivity (0.72 – 2.16 W/m·K) of HA¹⁷ and the wide particle size distribution (15 – 100 μ m) of the powders used, which made the cores of the larger particles difficult to melt even if the heat content increased.

On the other hand, as the SOD increased, the temperature of the substrate decreased and the cooling rate increased. The HA powders suffered more melting and dehydroxylation at longer



(a) SOD = 80 mm



(b) SOD = 160 mm

Figure 2. XRD patterns of HA coatings sprayed at different spray power levels and stand-off distances (a is α -TCP, β is β -TCP, T is TTCP, * is CaO and all other peaks belong to HA)

SOD. Thus, more melted portions of HA particles solidified into ACP phase and the crystallinity significantly decreased. Another important reason for the decrease of crystallinity at longer SOD is that some of the unmelted particles were blown away before they reached the substrate, which can be evidenced by the fact that the deposition efficiency at 160 mm SOD was only around 60% of that at 80 mm SOD.

Effects on Purity. The impurity phases in plasma sprayed HA coatings can be divided into two types: calcium phosphate (TCP and TTCP) impurity and CaO impurity. A main concern is their different effects on the biological responses of HA coatings. All the TCP and TTCP phases are reported to be biocompatible and dissolvable in body fluids.¹⁸ The only difference is that they have a higher dissolution rate than HA, but lower than the ACP,¹⁹ which is in the order of

(fast) ACP \gg TTCP $>$ α -TCP $>$ β -TCP \gg HA (slow)

On the other hand, CaO phase has no biocompatibility. It is considered to be the most detrimental phase following implantation because of its high reactivity in the presence of water.²⁰

The decomposition of the HA during the plasma spray process can be explained using the related CaO-P₂O₅-H₂O phase diagram²¹ with the temperature-time exposure experience of the HA powders and their cooling rate. The following steps have been suggested by de Groot et al.^{22,14} HA decomposed to form α -TCP and TTCP phases at high temperature, around 1325-1550°C which increased with an increase of the partial water pressure.¹³ The phase equilibrium equation²³ can be expressed as:



Some of the α -TCP then transformed at about 1100°C to β -TCP which is a stable TCP phase at room temperature. The TTCP phase would further decompose to form HA and CaO if a high heat content was involved.

As shown in Fig. 4, the percentage of all impurity phases increased with an increase of spray power, while the CaO percentage increased more significantly than TCP and TTCP. This occurs because more HA powder melted and decomposed as the plasma temperature increased at higher power. As well, the powders were more dehydroxylated at higher temperature, which decreased the decomposition temperature of HA to α -TCP and TTCP. The higher heat content at higher power also caused further decomposition of TTCP to HA and CaO. The impurity percentage did not exhibit a significant increase when the spray power was increased from 35 kW to 42 kW, which can be explained in a similar fashion as for the crystallinity.

It was reported in Yang et al's work¹⁴ that the SOD variables had no influence on the formation of impurity phases. In the present work, however, when the SOD increased from 80 mm to

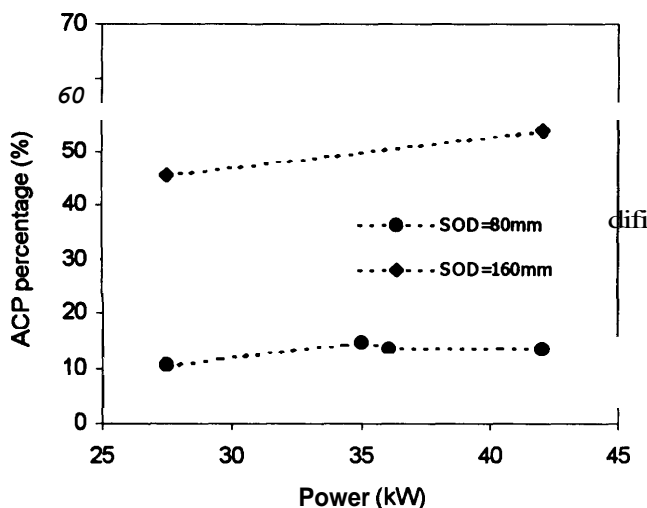
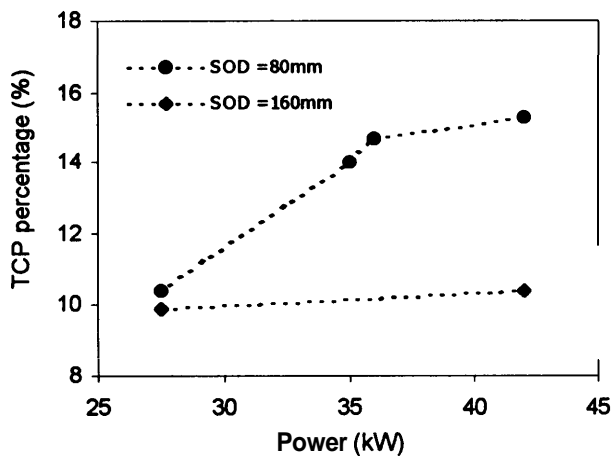
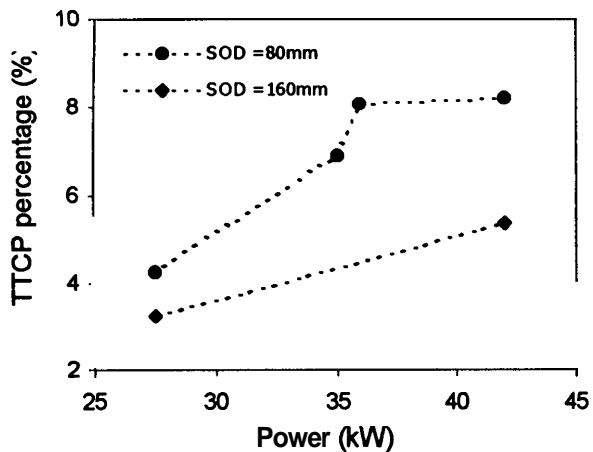


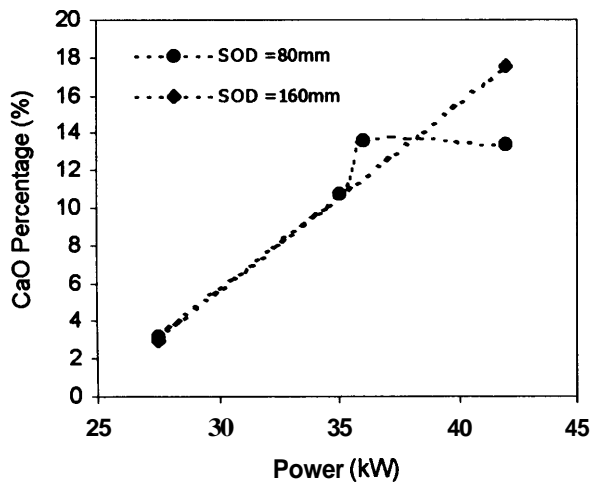
Figure 3. Effects of spray power and SOD on the crystallinity of HA coatings



(a) TCP percentage



(b) TTCP percentage



(c) CaO percentage

Figure 4. Effects of spray power and SOD on the purity of HA coatings

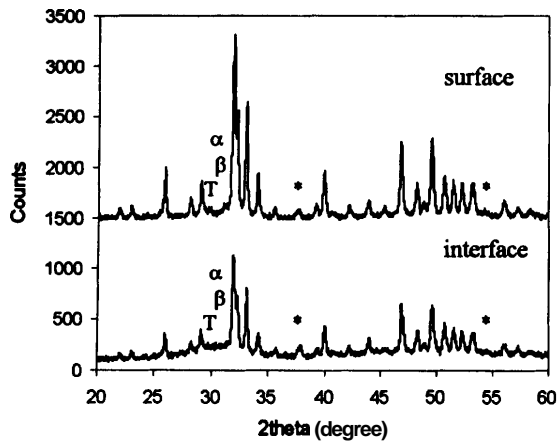
160 mm, the percentage of TCP and TTCP decreased while the CaO percentage increased, which is more obvious at higher spray power. The reason for this behavior is that although HA powders suffered more melting, decomposition and dehydroxylation at longer SOD, due to the higher cooling rate, most of the melted HA became ACP phase. Also, the higher cooling rate limited the short-range diffusion for the decomposition of HA to α -TCP and TTCP at higher temperature; while HA decomposed directly to the low-temperature impurity phases (i.e. CaO and β -TCP). This can also explain the results that at longer SOD, the percentage of both TCP and TTCP did not increase significantly when the spray power increased, while the CaO percentage reached the highest value when both the spray power and SOD were the highest. It shall be noted that, although also a low-temperature phase, the β -TCP percentage (included in TCP percentage here) did not exhibit the same trend with the spray parameters as CaO. A possible reason is the loss of the P_2O_5 group during the spray process. This phenomenon has been found to be related to the original powders and will be investigated in the future.

Phase distribution. As shown in Fig. 5, in all four extreme spray power/SOD combinations, the intensity of the overall HA peaks is evidently lower while the amorphous hump is more obvious in the XRD patterns of the interface than that of the surface of the HA coatings. For the impurity phases, the CaO peak is clearly higher in the XRD pattern of the interface than that of the surface, while the peaks of TCP and TTCP do not show obvious differences.

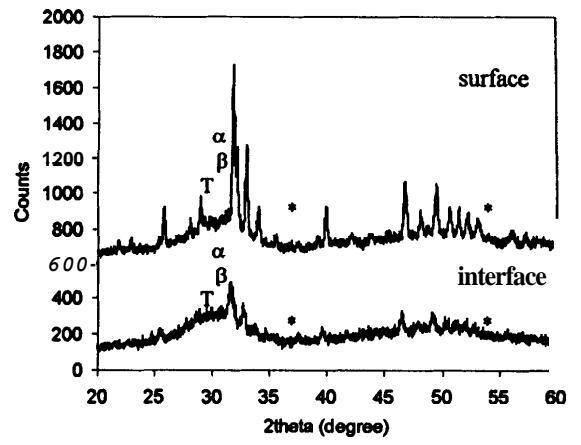
The difference of the crystallinity and the purity in the surface and the interface of the HA coating was also evaluated using the same quantitative analysis method introduced before. No significant difference (although some changes in the overall peak counts) was found between the XRD patterns of the surfaces of the HA coatings with the substrate and the peel-off HA coatings that were sprayed with the same parameters; i.e., the XRD pattern of the HA coating surface was not obviously influenced with respect to the coating thickness.

Figure 6 compares the crystallinity between the surface and the interface of the HA coatings. The ACP percentage was higher in the interface of the HA coating in all four extreme cases. This result is consistent with previous studies.^{15,24} During the plasma spraying process, the cooling rate of the first lamella was controlled by rapid heat dissipation to the metallic substrate. As the HA coating thickness increases, the cooling rate becomes much smaller because the thermal conductivity of HA ($\sim 0.72 - 2.16 \text{ W/m}\cdot\text{K}$)¹⁷ is much lower than that of metals (in our case, mild steel $\sim 20 - 60 \text{ W/m}\cdot\text{K}$), and this results in more recrystallization when the melt impacted onto the substrate. Thus, the ACP percentage was much higher at the coating interface.

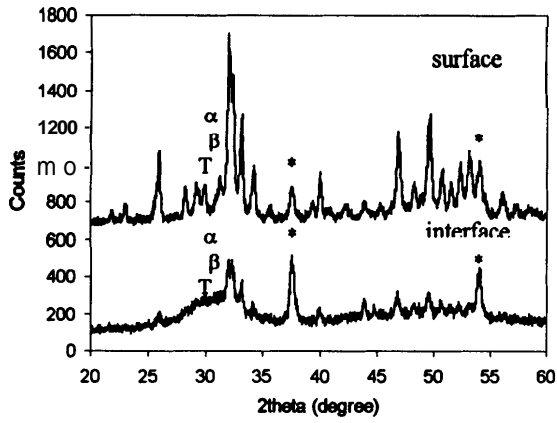
The percentage of impurity phases in the surface and the interface of HA coatings is shown in Fig. 7. The percentage of both TCP and TTCP was lower in the interface than at the surface. On the other hand, the CaO percentage was higher in the interface and the difference was more significant when SOD was shorter. This can be explained as before; i.e., the higher cooling rate at the beginning of spraying led to the formation of more ACP phase and limited the short-range diffusion for the decomposition of HA to α -TCP and TTCP at higher temperature. Instead, HA decomposed directly to the low-temperature phases (CaO and β -TCP). The



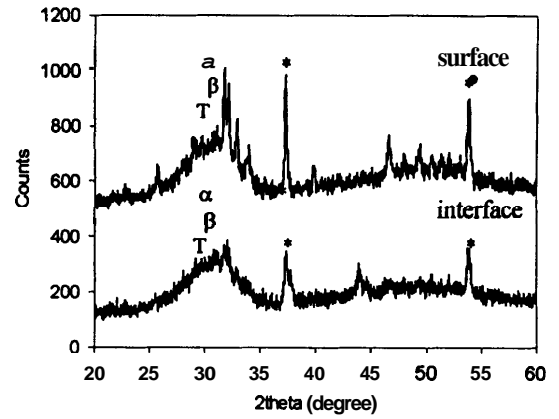
(a) 27.5 kW / 80 mm



(b) 27.5 kW / 160 mm



(c) 42 kW / 80 mm



(d) 42 kW / 160 mm

Figure 5. XRD patterns of **surface** and **interface** of HA coatings (a is α -TCP, β is β -TCP, T is TTCP, * is CaO and all other peaks belong to HA)

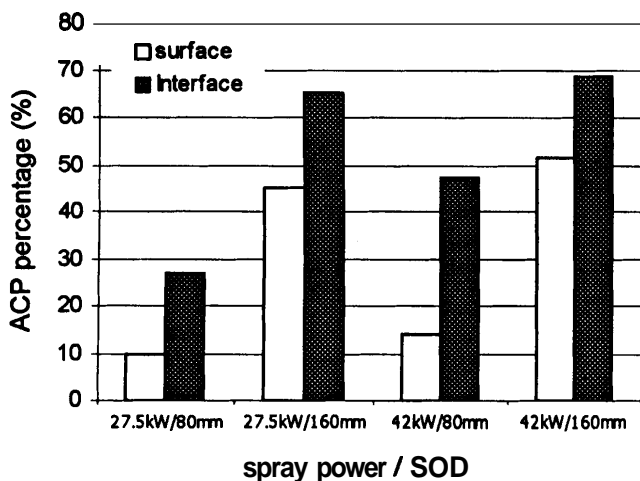
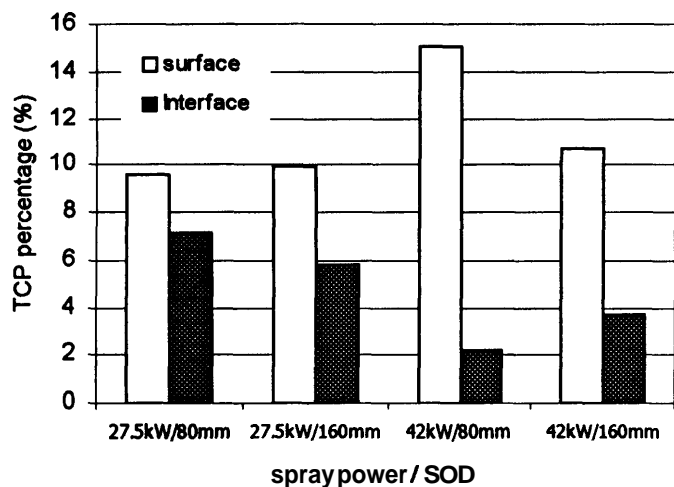


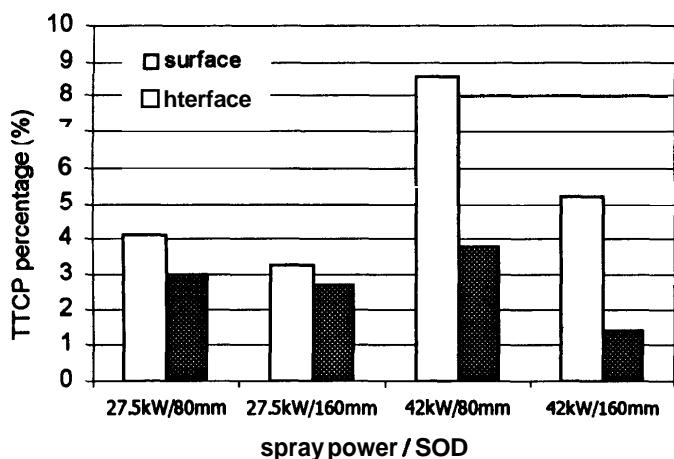
Figure 6. Comparison of crystallinity between surface and interface of HA coatings

significant difference at shorter SOD is due to the higher difference in cooling rate between the beginning and the end of spraying at shorter SOD.

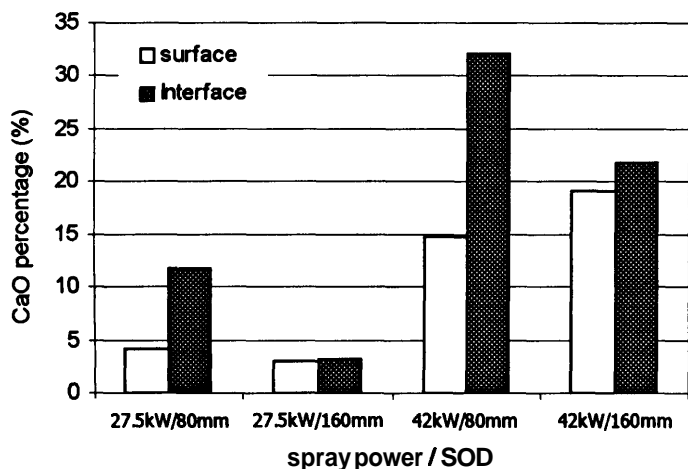
Summary. The effects of various spray **parameters** on phase formation and distribution within HA coatings can be explained using the temperature-time exposure experiences of HA powders and their cooling rate in the spraying process as well as the **CaO-P₂O₅-H₂O** phase diagram. In the present study, the effects of spray power can be attributed to the temperature experience while the effects of SOD are related to the residence time of the HA powders in the **plasma**. This can be summarized in Fig. 8. For example, track 1 **illustrates** the processes that occur when the spray power **increased**. In this instance, HA powders were exposed at higher temperature; **thus** more powders were melted, decomposed-and dehydroxylated. Also, the cooling rate increased. **All** these factors led to the lower crystallinity and higher impurity in HA coatings. On the other hand, when the SOD increased (track 2), HA powders were subjected to a high temperature for a longer time; thus more melting, decomposition and dehydroxylation occurred. The cooling rate decreased at longer time. However, as the substrate



(a) TCP percentage



(b) TTCP percentage



(c) CaO percentage

Figure 7. Comparison of impurity between **surface** and interface of HA coatings

temperature was much lower at longer SOD, the actual cooling rate increased a lot at longer SOD. This higher cooling rate and lower deposition efficiency (DE) at longer SOD contributed much to the lower crystallinity and higher **CaO** percentage of HA coatings. The lower crystallinity and higher CaO percentage at the interface of the HA coating were also the result of the much higher cooling rate at the metallic substrate at the beginning of spraying, as shown by track 3 in Fig. 8.

Conclusions

The effects of spray power and SOD on the crystallinity and the purity of the plasma sprayed HA coatings and phase distribution in the surface and the interface of HA coatings were systematically studied in this paper. The following conclusions can be drawn from the above analysis.

- (1) Both crystallinity and purity of the HA decreased **after** plasma spraying. The impurity phases included **tricalcium** phosphate (α -TCP, β -TCP), **tetracalcium** phosphate (TTCP) and calcium oxide (**CaO**), which were due to the decomposition of HA.
- (2) The crystallinity of HA coatings decreased with increasing spray power and SOD. The impurity percentage increased with the spray power. The percentage of **TCP** and **TTCP** **decreased** with the SOD while the CaO percentage increased, which is more obvious at higher spray power. All these effects can be explained using the temperature-time exposure experience of HA powders and their cooling rate during the spray process as well as the **CaO-P₂O₅-H₂O** phase diagram. The percentage of CaO was **significant** when both the spray power and the SOD were higher, which should be avoided in producing HA coatings.
- (3) The **crystallinity** was **significantly** lower at the interface than at the **surface** of the HA coatings. The percentage of **TCP** and **TTCP** is lower in the interface than at the surface, while the **CaO** percentage is greater, especially at shorter SOD. **All** these effects were due to the higher cooling rate at the beginning of spraying.

Acknowledgments

This work is supported under NSF-MRSEC DMR grant number 9632570. The authors would also like to thank **Christienne E. Mancini** and Matthew R. Gold for their assistance.

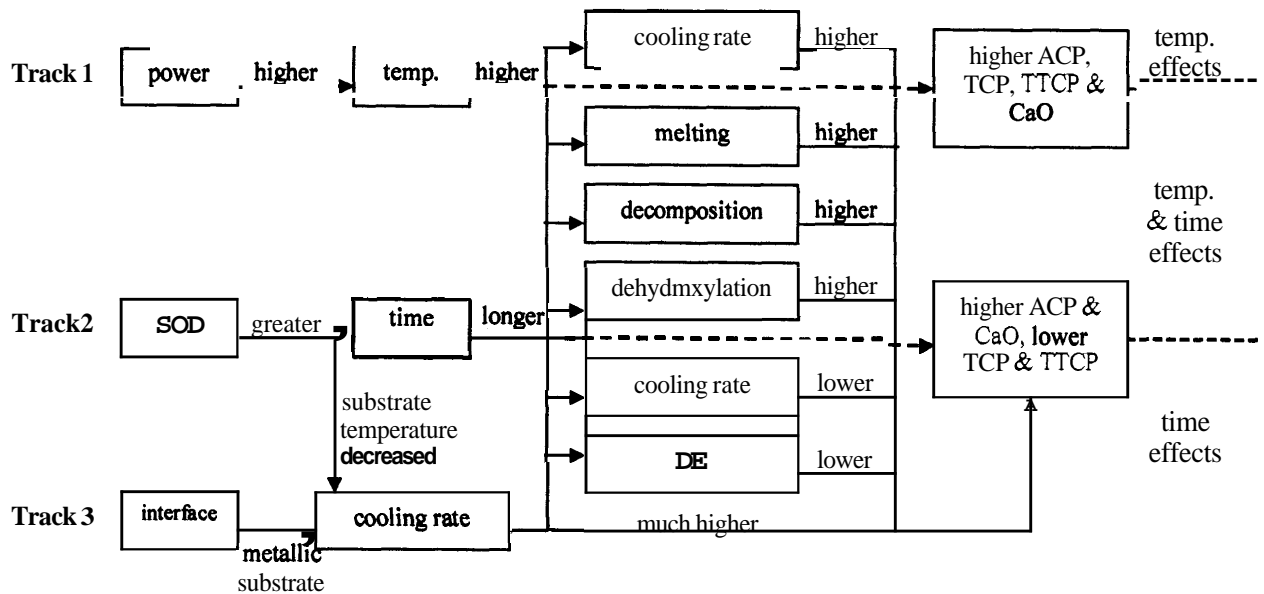


Figure 8. Relationship between spray parameters and phase formation and distribution of HA coatings
(The factors above and below the dashed line are respectively caused by the change of temperature and time, while the factors between the dashed line are caused by both.)

References

- C.C. Berndt, G.N. Haddad, A.J.D. Farmer and K.A. Gross, "Thermal spraying for bioceramic applications," *Mater. Forum*, 14, 161-73 (1990)
- Y. Cao, J. Weng, J. Cheng, J. Feng, Z. Yang and X. Zhang, "Water vapour-treated hydroxyapatite coatings after plasma spraying and their characteristics," *Biomaterials*, 17, 419-24 (1996)
- Y.C. Tsui, C. Doyle, T.W. Clyne, *Biomaterials*, "Plasma sprayed hydroxyapatite coatings on titanium substrates Part 1: Mechanical properties and residual stress levels," 19, 2015-29 (1998)
- B.C. Wang, E. Chang, T.M. Lee and C.Y. Yang, "Changes in phases and crystallinity of plasma-sprayed hydroxyapatite coatings under heat treatment: A quantitative study," *Journal of Biomedical Materials Research*, 29, 1483-92 (1995)
- K.A. Gross and C.C. Berndt, "Optimization of spraying parameters for hydroxyapatite," in *Proc. 2nd Plasma-Technik Symposium*, 3, ed. S. Blum-Sandmeier, H. Eschnauer, and P. Huber, Plasma-Technik AG, Wohlen, Switzerland, 159-70 (1991)
- J.C. Elloit, *Structure and Chemistry of the Apatites and Other Calcium Orthophosphates*, p 6, Elsevier, Amsterdam (1994)
- P. Ducheyne, S. Radin and L. King, "The effect of calcium phosphate ceramic composition and structure on in vitro behavior I. Dissolution," *J. Biomed. Mater. Res.* 27, 25-34 (1993).
- K.A. Gross, C.C. Berndt, D.D. Goldschlag and V.J. Iacono, "In vitro changes of hydroxyapatite coatings," *Int. J. Oral & Maxillofac Implants*, 12, 589-97 (1997)
- J. Weng, Q. Liu, J.G.C. Wolke, X. Zhang and K. de Groot, "Formation and characteristics of the apatite layer on plasma-sprayed hydroxyapatite coatings in simulated body fluid," *Biomaterials*, 18, 1027-35 (1997)
- Selected Powder Diffraction Data for Minerals, 1st Ed. Joint Committee on Powder Diffraction Standard (JCPDS), Philadelphia, PA (1974)
- J.P. LeGeros, R.Z. LeGeros, A. Burgess, B. Edwards and J. Zitelli, "X-ray diffraction method for the quantitative characterization of calcium phosphate coatings," in *Characterization and Performance of Calcium Phosphate Coatings for Implant*, ASTM STP 1196, ed. E. Horowitz and J. E. Parr, ASTM, Philadelphia, PA, p. 33-42 (1994)
- B.C. Wang, E. Chang, T.M. Lee and C.Y. Yang, "Changes in phases and crystallinity of plasma-sprayed hydroxyapatite coatings under heat treatment: A quantitative study," *J. Biomed. Mater. Res.*, 29, 1483-92 (1995)
- R. McPherson and N. Gane, "Structural characterization of plasma-sprayed hydroxyapatite coatings," *J Mater. Sci. Mater. Med.*, 6, 327-34 (1995)
- C.Y. Yang, B.C. Wang, E. Chang and J.D. Wu, "The influence of plasma spraying parameters on the characteristic of hydroxyapatite coatings: a quantitative study," *J. Mater. Sci. Mater. Med.*, 6, 249-57 (1995)
- K.A. Gross, *The Amorphous Phases in Hydroxyapatite Coatings*, p 175, Ph.D. thesis, State University of New York at Stony Brook, Stony Brook, New York (1995)

- ¹⁶ B.D. **Cullity**, Elements of X-ray **Diffraction**, 2nd Edition, p 415, Addition-Wesley Publishing Co., Reading, Massachusetts (1978)
- ¹⁷ T.W. Clyne and Y.C. **Tsui**, "The effect of intermediate layers on residual stress distributions and debonding of sprayed thermal **barrier** coatings," in 3rd **Int Symp** on Structural and Functional Gradient Materials, ed. B. **Ilschner**, **PPUR** 129-36 (1994)
- ¹⁸ **S.R Radin** and P. Ducheyne, "Plasma spraying induced changes of calcium phosphate ceramic characteristics and the effect on in **vitro** stability," *J. Mater. Sci. Mater. Med.* 3, 33-42, (1992)
- ¹⁹ R. Z. **LeGeros**, "Biodegradation and **bioresorption** of Calcium phosphate ceramics," *Clin. Mater.*, **14**, 65-68, (1993)
- ²⁰ A. **Slosarczyk**, C. **Paluszkiewicz**, M. **Gawlicki** and Z. **Paszkiwicz**, "The FTIR spectroscopy and QXRD studies of calcium phosphate based materials produced from the powder precursors with different Ca/P ratios," *Ceram. Intern.*, 23, 297-304, (1997)
- ²¹ P.V. **Riboud**, "Composition and stability of apatites in the system **CaO-P₂O₅-Iron oxide-H₂O** at high temperature," *Ann. Chim.* **8**, 381-90 (1973)
- ²² K. de **Groot**, C.P.A.T. **Klein**, J.G.C. **Wolke** and J.M.A. de **Blieck-Hogervorst**, "Plasma-sprayed coatings of calcium phosphate," in CRC Handbook of **Bioactive** Ceramics, ed. T. **Yamamuro**, L.L. Hench and J. Wilson, CRC Press, Boca **Raton**, MA, 3-16 (1990)
- ²³ **W. Van Raemdonck**, P. Ducheyne and P. De **Meester**, "Calcium phosphate ceramics," in Metal and Ceramic **Biomaterials**, v. 2, ed. P. Ducheyne and W. Hasting, CRC Press, Boca **Raton**, FL, p 149 (1984)
- ²⁴ H. Ji, C.B. **Ponton** and P.M. Marquis, "Microstructural characterization of **hydroxyapatite** coating on titanium," *J. Mater. Sci. Mater. Med.*, 3,283-87 (1992)